

# Electronic Properties of Hybrid Zinc Oxide–Oligothiophene Nanostructures

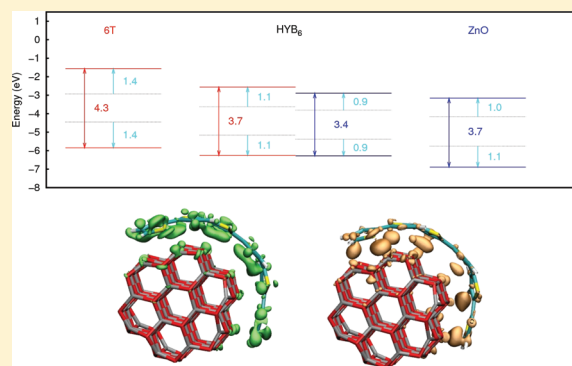
Claudia Caddeo,<sup>\*,†,‡</sup> Giuliano Mallocci,<sup>‡</sup> Gian-Marco Rignanese,<sup>§</sup> Luciano Colombo,<sup>†,‡</sup> and Alessandro Mattoni<sup>‡</sup>

<sup>†</sup>Dipartimento di Fisica Università di Cagliari and <sup>‡</sup>Istituto Officina dei Materiali (CNR-IOM), Unità Cagliari, Cittadella Universitaria, I-09042 Monserrato (Ca), Italy

<sup>§</sup>Institute of Condensed Matter and Nanosciences (IMCN), Université Catholique de Louvain, NAPS- Chemin des étoiles 8 bte L7.03.01, 1348 Louvain-la-Neuve Belgium

## S Supporting Information

**ABSTRACT:** Using density functional theory in combination with model potential molecular dynamics, we study hybrid systems consisting of oligothiophene molecules with increasing chain length (two, four, and six rings) adsorbed onto a ZnO nanoparticle model. We investigate the energetics of adhesion and the morphological features at the curved interface. We compute the energy-level alignment taking many body effects into account within the  $\Delta$ SCF approach. Our results show that, as a consequence of the local curvature of the interface, the electronic coupling between the organic and inorganic component affects the energy-level alignment in all systems, making it less favorable for charge separation. In particular, the energy-level alignment for sexithiophene on the ZnO curved nanoparticle does not lead to a type-II junction with staggered band gaps, contrary to what was recently found for sexithiophene on a flat (10 $\bar{1}0$ ) ZnO surface. Although the limited size (and hence the large curvature) of the nanoparticle does not allow us to make a general statement, this indicates a trend that is valid for systems in which quantum confinement effects are important. As a side result of our study, we propose a simple practical model to predict the energy-level alignment in hybrid systems, which gives consistent results compared to  $\Delta$ SCF.



## 1. INTRODUCTION

Hybrid organic/inorganic systems have attracted great interest as a new class of materials with high technological impact in molecular electronics,<sup>1,2</sup> textiles,<sup>3</sup> bioengineering,<sup>4</sup> and photovoltaics.<sup>5</sup> Indeed, they can combine the advantages of both organic and inorganic materials while being quite easy to fabricate. In particular, hybrid solar cells formed by a metaloxide (the electron acceptor) and a conjugated polymer (the electron donor) are a cheap and environmental-friendly potential alternative to standard Si-based systems. These can be produced as phase-separated bilayers,<sup>6</sup> but the best efficiency is reached for bulk heterojunction architectures,<sup>5</sup> in which, for example, the inorganic electron acceptor consists of nanometer-sized particles dispersed in an electron donor polymer matrix. Such a two-phase intermixing increases the effective interfacial area and improves charge separation. Nevertheless, photoconversion efficiency is still low at the moment (around 2%),<sup>5</sup> and lots of research is currently in progress to improve it.

Among the various materials that can be used as an electron acceptor, zinc oxide is very promising. It has high electron mobility,<sup>7</sup> it is cheap, biosafe, and easily synthesizable in nanostructures.<sup>8,9</sup> Furthermore, the electronic properties of such nanostructures can be tuned by controlling their size and shape.<sup>10</sup> The organic electron donor can either be a long chain

polymer, such as poly(3-hexylthiophene) (P3HT<sup>5</sup>), or an oligomer, as for example sexithiophene (6T).<sup>11</sup> More specifically, thiophene derivatives have shown to be very promising in ZnO-based bulk heterojunction solar cells.<sup>12,13</sup> In addition, 6T has the advantage of giving rise to highly ordered crystalline structures,<sup>14,15</sup> which offer better conducting properties than disordered crystals.<sup>16</sup> Furthermore, recent ultraviolet photoelectron spectroscopy measurements of 6T on ZnO surfaces show that such a heterostructure is suitable for photovoltaics.<sup>11</sup>

The performances of hybrid systems depend on some basic atomic-scale features of the device. In particular, the electronic energy-level alignment at the interface is a fundamental property for designing systems with the desired optoelectronic behavior. A critical requirement for photovoltaic applications is that the interface corresponds to a type-II (staggered) junction in order to get an efficient charge separation. Accurate characterization of interfaces is still an open issue due to the difficulty of measuring properties at the nanometric scale. This challenge makes atomistic simulations an important tool for

Received: December 20, 2011

Revised: March 2, 2012

Published: March 5, 2012

understanding and predicting the interfacial morphology and optoelectronic properties.

Model potential molecular dynamics (MPMD) has been successfully applied to study morphological properties at the interface, as atomic scale organization of molecules.<sup>17,18</sup> *Ab initio* calculations, on the other hand, yield information on the electronic structure and related properties, such as adsorption,<sup>19</sup> optical absorption spectra,<sup>20</sup> or energy-level alignment.<sup>21</sup> In particular, density functional theory (DFT)<sup>22</sup> has been widely used to study energy-level alignment and charge transfer in fully organic solar cells,<sup>23,24</sup> and adhesion of P3HT<sup>25</sup> and 6T<sup>26</sup> molecules on a planar ZnO (10 $\bar{1}$ 0) surface. It has also been applied to standalone ZnO clusters<sup>27–29</sup> and small molecules adsorbed on ZnO clusters,<sup>30–32</sup> but, to our knowledge, there is no theoretical study on hybrid structures formed by a ZnO nanocluster and thiophene derivatives. Nevertheless, DFT (which is, in its most basic formulation, a ground-state theory) likely provides results on energy gaps and electronic levels alignment that strongly depend on the choice of the exchange/correlation functional. For instance, standard functionals suffer from the well-known band gap problem.<sup>33,34</sup> Better agreement with experiments is usually obtained using hybrid functionals, but these require significantly higher computational load,<sup>26</sup> and their reliability cannot be assessed *a priori*.<sup>35,36</sup> In contrast, the so-called Hedin's GW approximation<sup>37</sup> gives excellent results for many materials (see, e.g., refs 38 and 39); however, despite recent progress,<sup>39,40</sup> GW calculations are still prohibitively expensive for complex systems with a large number of atoms. For finite systems, the so-called  $\Delta$  self-consistent field ( $\Delta$ SCF) approach<sup>41</sup> can successfully be used to determine the quasiparticle (QP) energy levels. This approach has proven to give good results when applied to bound one-electron excitations and ionization energies of atoms and molecules,<sup>41</sup> and it will be used in the present work. Its accuracy has already been investigated,<sup>42–44</sup> even though a comparison with GW calculations would be highly desirable.

The nanostructurization of ZnO can have an impact on the physical properties of the hybrid systems. In particular, the curvature of the surface can alter the morphology of the interface. For example, in a previous extensive MPMD study on ZnO-P3HT bulk heterojunctions, we found that helical arrangements of the polymer chain occur on ZnO nano-needles.<sup>45</sup>

In this work, we consider a hybrid nanostructure consisting of an oligothiophene and a ZnO cluster of 120 atoms. Clusters of this specific size have been produced by laser ablation<sup>46</sup> and proven to be particularly stable. We focus in particular on the hexagonal wurtzite rod-like structure, which is here considered a good model of larger nanocrystals used in photovoltaics applications.<sup>13</sup> As for the chosen electron donor, we consider a *n*-thiophene rings oligomer (*n*T, with *n* = 2,4,6). We adopt a hierarchical combination of MPMD and DFT, providing a numerically efficient computational protocol to identify the minimum energy configurations of the hybrids. The  $\Delta$ SCF scheme is applied to study the energy-level alignment of the hybrid interfaces considered. From the methodological standpoint, we additionally propose a simple model for studying hybrid interfaces that only requires the  $\Delta$ SCF calculation on their isolated components. For the specific case of ZnO-6T, we find that the interface is less favorable for charge separation at variance with the case of planar ZnO surface.<sup>26</sup>

## 2. COMPUTATIONAL FRAMEWORK

In order to generate models of hybrid nanosystems, we perform MPMD simulations combined with DFT calculations through the following multistep procedure. We first consider the different building blocks of the hybrid systems (ZnO and *n*T) separately, and fully relax their structures at the DFT level. The considered ZnO cluster has hexagonal cross-section along the [0001] direction, and exhibits six (10 $\bar{1}$ 0) nonpolar facets. It has been obtained by cutting and relaxing a portion of bulk ZnO. It is represented in Figure 1 together with the relaxed *n*T

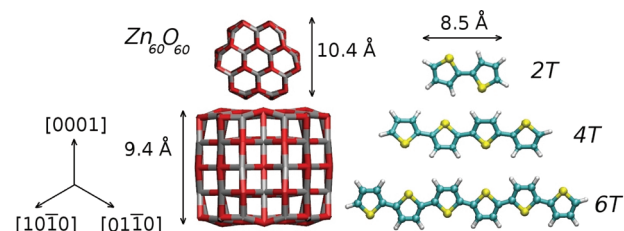


**Figure 1.** Left: top and side view of the Zn<sub>60</sub>O<sub>60</sub> nanocluster. Right: View of the planar oligomers. In all figures, red is oxygen, gray is zinc, cyan is carbon, yellow is sulfur, and white is hydrogen.

molecules. Three hybrid systems (hereafter labeled as HYB<sub>2</sub>, HYB<sub>4</sub>, and HYB<sub>6</sub>) are then obtained by merging the ZnO cluster and 2T, 4T, and 6T separately. Their structures are first relaxed using MPMD keeping the positions of all the ZnO atoms fixed at the DFT geometry, while the polymer is allowed to move and relax following long-range electrostatic and van der Waals forces. It is known that the thiophene derivatives adhesion on the ZnO (10 $\bar{1}$ 0) surface is anisotropic: in ref 45 we found that, for a P3HT molecule, the lowest energy configurations are obtained when the polymer is placed with its backbone parallel or perpendicular to the [0001] direction. Thus, here we start from the two preferred orientations of the oligomer, and then we perform a 100 ps-long MPMD simulation at low temperature, followed by a conjugate-gradient optimization. We find the same minimum for both the configurations, showing that the initial guess does not influence the final result. Finally, the MPMD resulting structures are fully relaxed at the DFT level. Ground-state DFT calculations are performed with the quantum chemistry program package turbomole.<sup>47</sup> In all calculations, the PBE exchange-correlation functional<sup>48</sup> is used to model the exchange-correlation energy. The electronic wave functions are represented using a Gaussian orbital basis set of split valence triple- $\zeta$  quality augmented with polarization functions (TZVP).<sup>49</sup> In all cases, the resolution of identity approximation is adopted for computing the electronic Coulomb interaction:<sup>50</sup> this usually leads to a more than 10-fold speedup of the calculations, without sacrificing accuracy. In addition, the multipole accelerated resolution of identity approximation<sup>51</sup> is used, enabling even more efficient calculations. In each SCF cycle, we require the energy to be converged within  $3 \times 10^{-6}$  eV, and the grid for numerical evaluation of the exchange-correlation operator is set to medium size.<sup>52</sup> The dispersive van der Waals interactions are included by applying the Grimme correction.<sup>53,54</sup> Adhesion energies are corrected for the basis-set superposition error using the counterpoise method.<sup>55</sup>

As for the MPMD simulations, they are all performed using the DL\_POLY 3 code.<sup>56</sup> The *n*Ts are described by the AMBER force field,<sup>57</sup> that includes either bonding (stretching, bending,

and torsional) and nonbonding (van der Waals and Coulomb) contributions. The standard AM1-CM2 method<sup>58</sup> is applied to calculate the atomic partial charges for the *n*Ts. The ZnO–polymer interactions are described as a sum of electrostatic and dispersive contributions (of Lennard-Jones type), with parameters taken from the Amber database.<sup>57</sup> All the electrostatic contributions are computed by the Ewald sum method with real space cutoff,  $\rho_c = 8 \text{ \AA}$ . Partial charges for ZnO are taken from Kullkarni et al.<sup>10</sup> The atomic trajectories are calculated using the velocity Verlet algorithm with a time step as small as 0.5 fs. Temperature is controlled by a Berendsen thermostat with a relaxation constant of  $f = 0.5 \text{ ps}$ .

QP energies are computed directly as total-energy differences in the framework of the  $\Delta$ SCF scheme.<sup>41</sup> Since all the electronic excitations considered here are easily described in terms of isolated single-particle transitions, the application of the  $\Delta$ SCF method is fully justified (see, e.g., the work of Onida et al.<sup>37</sup>). In particular, for an *N* electrons system, any empty (occupied) level is corrected by calculating the total energy  $E_{N-1}$  ( $E_{N+1}$ ) of the same system with an additional (missing) electron in it. Specifically, an empty (occupied) level is corrected by replacing its corresponding DFT eigenvalue with  $E_{N+1} - E_N$  ( $E_N - E_{N-1}$ ).

### 3. RESULTS AND DISCUSSION

**3.1. Morphology and Energetics.** We first perform a PBE/TZVP optimization of  $\text{Zn}_{60}\text{O}_{60}$ , with 2T, 4T, and 6T separately. During the geometry optimization of  $\text{Zn}_{60}\text{O}_{60}$ , the Zn–O double layers merge into single layers containing both Zn and O atoms. This phenomenon has been observed before,<sup>59</sup> and it is due to the presence of polar O-terminated and Zn-terminated surfaces that give rise to an electric field in the cluster.<sup>60</sup> Thus, the Zn and O ions with opposite charges move toward a common plane to find a relatively stable state. This modification affects only the planes perpendicular to the *c* axis, while the hexagonal cross-section is preserved. Starting from the separate optimized geometries, we follow the combined MPMD+DFT minimization procedure described in Section 2. The final optimized geometries of the three hybrids considered are shown in Figure 2. We notice that the optimal

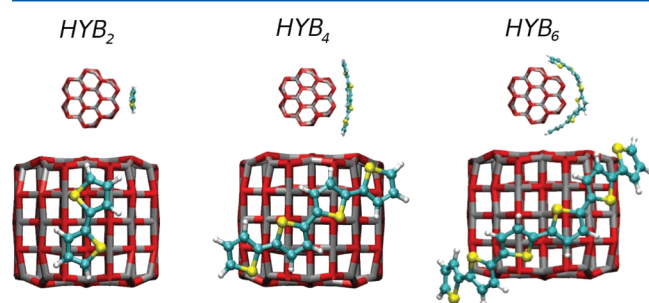


**Figure 2.** Top and side view of the three hybrids after the overall MPMD+DFT relaxing procedure.

position of the *n*T with respect to the nanocrystal is different from that obtained for P3HT on a flat  $(10\bar{1}0)$  ZnO surface.<sup>45</sup> In particular, the angle formed between the *n*T backbone and the  $[0001]$  direction of the nanocrystal increases at increasing *n*T length. This is a size effect: the organic molecules bend in order to maximize the interaction with the nanocrystal, while this distortion is not needed in the case of a flat surface.

The minimum energy structures in Figure 2 do not differ significantly from their classical counterparts with the exception

of  $\text{HYB}_6$ . In this case, in the final MPMD configuration, the 6T does not wrap around the nanocrystal. This can be attributed to a too large stiffness of the molecule as described by the MP. After relaxing the hybrid structures, we calculate the adhesion energy  $U_{\text{adh}}$  of the *n*T on the ZnO nanocluster, defined as

$$U_{\text{adh}} = U_{\text{hyb}} - U_{\text{ZnO}} - U_{n\text{T}} \quad (1)$$

where  $U_{\text{hyb}}$ ,  $U_{\text{ZnO}}$ , and  $U_{n\text{T}}$  are the total energies of the hybrid system, the optimized ZnO nanocluster, and the straight optimized *n*T, respectively.

The computed  $U_{\text{adh}}$  and the stacking distance  $d_{\text{stack}}$  between the center of the molecule and the nanocrystal facet are reported in Table 1 (total). In order to separately account for

**Table 1.** Adsorption Energies (Values in eV) and Stacking Distances (Values in  $\text{\AA}$ )

	total			nondispersive		
	$U_{\text{adh}}$	$U_{\text{adh}}/\text{mon}$	$d_{\text{stack}}$	$U_{\text{adh}}$	$U_{\text{adh}}/\text{mon}$	$d_{\text{stack}}$
$\text{HYB}_2$	1.31	0.65	2.7–2.9	0.45	0.22	2.8–3.2
$\text{HYB}_4$	1.34	0.34	2.4–2.9	0.29	0.07	2.6–3.1
$\text{HYB}_6$	1.96	0.33	2.8–3.0	0.29	0.05	2.9–3.3

dispersive and covalent contributions to the adhesion energy, we performed again all the calculation neglecting the dispersive forces. The results are reported in Table 1 as the nondispersive case. The effect of dispersive interactions on the geometries is to bend the organic molecule so as to adapt to the local curvature of the nanocrystal. This effect is larger for the longest molecules (4T and especially 6T), while it is negligible for the  $\text{HYB}_2$  system. The structures obtained by neglecting the dispersive interactions can be found in the Supporting Information. We conclude that the adhesion is mainly given by dispersive forces, since no chemical bond is formed between the organic molecule and the nanocluster. The total adhesion energy per monomer  $U_{\text{adh}}/\text{mon}$  is smaller than the experimental value of  $\sim 0.65\text{--}0.87 \text{ eV}$  for thiophene on a flat ZnO surface.<sup>61</sup> This is expected given several adhesion reduction effects such as polymer strain, anisotropy, and edges as described in ref 45. We also remark that the *n*T adhesion increases with *n*. At variance, when dispersion is not included, the adhesion converges to a constant value of about 0.3 eV. In this case, the molecule does not wrap the nanocrystal, and the adhesion is only due to the two central thiophene rings. The adhesion energy in this case agrees with the results reported in Sai et al.<sup>26</sup> for 6T on ZnO surface calculated without dispersion. As for the stacking distance, it is found to be approximately constant for all *n*T lengths. A longer distance is found when dispersive interactions are neglected. The calculated values are again consistent with those of ref 45 and are typical of a physisorption mechanism.

**3.2. Electronic Properties.** In order to study the energy-level alignment at the interface, four levels must be considered, i.e., the highest occupied molecular orbital (HOMO) and lowest unoccupied molecular orbital (LUMO) of the two components. These levels can be identified by examining both spatial distribution and energies of the molecular orbitals of the hybrid. The corresponding  $\Delta$ SCF corrected levels are shown in Figure 3 (middle). The levels of the separate components at the hybrid geometry are reported as well (left *n*T, right ZnO).

The interaction between the ZnO nanocluster and the *n*T molecule shifts the electronic levels of the separated

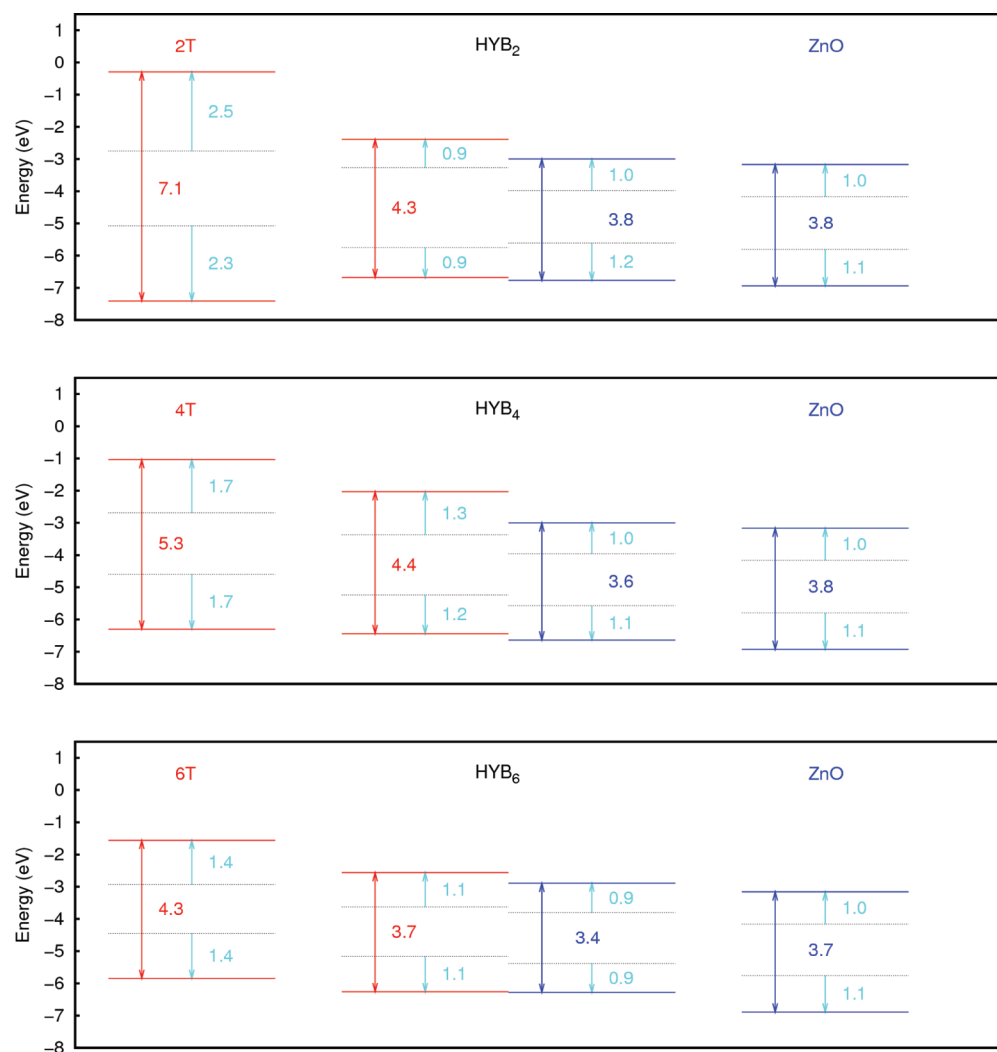


**Figure 3.** Energy-level alignment of the three hybrids considered as obtained with the  $\Delta$ SCF method; dashed lines correspond to the DFT levels.

components, with larger shifts for the  $n$ Ts (0.4–0.7 eV) as compared to  $\text{Zn}_{60}\text{O}_{60}$  (0.2–0.4 eV). These shifts can be attributed to an electronic coupling between the two components, which induces a charge displacement from the  $n$ T to the metaloxide. This effect has been also observed for other organic molecules adsorbed onto inorganic surfaces.<sup>62</sup> In Figure 4 we plot the difference between the electronic density of the interacting and noninteracting system. More specifically, the electronic densities of 2T, 4T, 6T, and  $\text{Zn}_{60}\text{O}_{60}$  at the geometry of the interacting configuration have been subtracted from the electronic density of the hybrid systems. Figure 4 shows that some charge is displaced from regions around the thiophene rings (green isosurfaces) to the region between the  $n$ T and the nanocrystal (orange isosurfaces). There is more charge displaced for  $\text{HYB}_2$  and  $\text{HYB}_6$  than for  $\text{HYB}_4$ , and this is reflected in the more pronounced levels shift observed for these systems (see Figure 3). We attribute this effect to the lower adhesion of the terminal rings of the 4T chain to the nanocrystal. In fact, this molecule is too long to accommodate entirely on the  $\text{Zn}_{60}\text{O}_{60}$  without bending its backbone (as the 2T), but too short to be flexible enough to wrap around the nanocluster as the 6T (see Figure 4).

Figure 3 shows that, for all the three hybrid systems studied, the energy-level alignment is unfavorable for holes transfer, as the HOMOs of the two moieties are almost coincident in all cases. Our results for  $\text{HYB}_6$  can be compared with those obtained by Sai et al.<sup>26</sup>

for the same 6T on a (10 $\bar{1}$ 0) ZnO planar surface, in which the alignment of type-II is preserved. The reduced offset observed in our calculations for  $\text{HYB}_6$  is a consequence of the nanostructuring of ZnO and the curvature of the molecule, which induce a different electronic coupling between the metaloxide and the organic molecule. This coupling shifts the original electronic levels of the separate moieties, producing an alignment that is detrimental for holes transfer. The present result suggests that, although the use of nanoparticles can be beneficial to have blends with large interface area, the nanocurvature of the interface can impact the electronic levels alignment. In a realistic solar cell, however, the nanoclusters are typically embedded in a oligothiophene matrix, and different configurations can be expected due to the interactions between oligothiophenes. Thus, deviations from our results are possible.

**3.3. Predictive Model for the QP Alignment.** Provided that the hybridization between the two systems is not too strong, the QP corrections in the hybrid ( $\Delta_i$ ) can be approximated using a simple model. Indeed, each state  $i$  can be associated with one of the components taken separately. Also, assuming that the screening is inversely proportional to the gap, we can write

$$(\Delta_i^{\text{sep}}/\text{gap}_{\text{KS}}^{\text{sep}}) \simeq (\Delta_i/\text{gap}_{\text{KS}})$$

where  $\Delta_i^{\text{sep}}$  is the QP correction for the component associated with the  $i$ th state taken separately, and  $\text{gap}_{\text{KS}}$  and  $\text{gap}_{\text{KS}}^{\text{sep}}$  are the

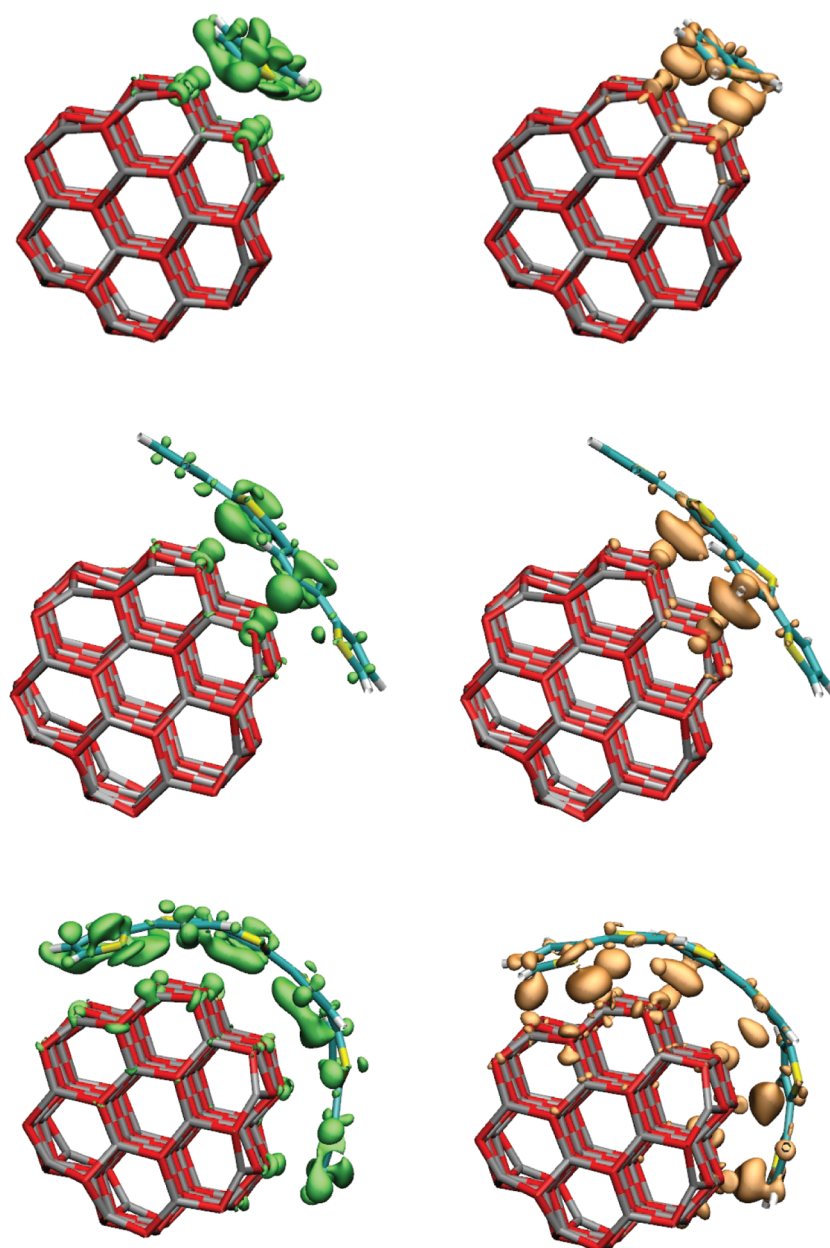


**Figure 4.** Difference density plots showing the displacements of electronic charge induced by the ZnO–*n*T interaction. Green isosurfaces (left panels) correspond to regions where the difference is negative, orange isosurfaces (right panels) where it is positive, showing that charge density moves from green regions to orange regions (isovalue equal to 0.001 e/a.u.).

**Table 2.** Comparison between the QP Levels as Obtained via  $\Delta$ SCF and the Model Described by Eq 2

		HYB <sub>2</sub>		HYB <sub>4</sub>		HYB <sub>6</sub>	
		model	$\Delta$ SCF	model	$\Delta$ SCF	model	$\Delta$ SCF
<i>n</i> T	HOMO	−7.1	−6.68	−6.4	−6.44	−6.3	−6.26
	LUMO	−1.9	−2.39	−2.3	−2.03	−2.5	−2.56
Zn <sub>60</sub> O <sub>60</sub>	HOMO	−6.7	−6.77	−6.5	−6.64	−6.3	−6.28
	LUMO	−3.0	−3.00	−3.2	−3.00	−3.0	−2.89
	gap	4.0	3.68	3.2	3.44	3.4	3.37

Kohn–Sham gaps calculated in the hybrid and in the separate systems, respectively. As a result, the QP energies of the hybrid can be simply written as

$$E_{i,\text{QP}} = \varepsilon_{i,\text{KS}} + \Delta_i = \varepsilon_{i,\text{KS}} + \left( \frac{g_{\text{P}}^{\text{KS}}}{g_{\text{A}}^{\text{KS}}} \right) \Delta_i^{\text{sep}} \quad (2)$$

As shown in Table 2 the results of the model are always qualitatively consistent with the full  $\Delta$ SCF calculation, with a better agreement at increasing system size. We remark that the SCF calculations of the hybrids involving the removal/addition of an electron from/to a level other than HOMO/LUMO are difficult since they converge slowly. The advantage of this

model is to allow the use of the results for the isolated components to obtain the QP levels, avoiding four single-point calculations on each hybrid system.

#### 4. CONCLUSIONS

We have presented a systematic theoretical study on hybrid systems composed by a  $\text{Zn}_{60}\text{O}_{60}$  hexagonal wurtzite nanocrystal and a oligothiophene molecule (bithiophene, quaterthiophene, and sexithiophene). We have performed ground-state structural relaxations combining MPMD and all-electrons DFT calculations. Starting from the DFT electronic structure, we have accurately evaluated the energy-level alignment between the organic and inorganic moieties by means of the  $\Delta\text{SCF}$  method. We have found that all the junctions are ineffective for charge separation at the interface, as a consequence of the nanostructurization of ZnO and the curvature of the molecule, which induce an electronic coupling between the organic and inorganic component. In particular, we have compared the case of  $\text{Zn}_{60}\text{O}_{60}$ -6T with the previously reported study of 6T on a flat (10 $\bar{1}$ 0) ZnO surface. While a type-II junction was found in the latter case, this staggered energy-level alignment is lost when the ZnO is nanostructured. Although this effect might be reduced for larger clusters, it definitely gives a trend for systems in which quantum confinement effects are important. From the methodological standpoint, we have additionally proposed a simple practical model that only requires one to apply the  $\Delta\text{SCF}$  method to the individual components of the hybrids. This model provides results consistent with those obtained via the full  $\Delta\text{SCF}$  for the composite systems.

#### ■ ASSOCIATED CONTENT

##### Supporting Information

In the Supporting Information we report some additional details on the calculations. This information is available free of charge via the Internet at <http://pubs.acs.org>

#### ■ AUTHOR INFORMATION

##### Corresponding Author

\*E-mail: [claudia.caddeo@dsf.unica.it](mailto:claudia.caddeo@dsf.unica.it)

##### Notes

The authors declare no competing financial interest.

#### ■ ACKNOWLEDGMENTS

This work has been funded by the Italian Institute of Technology (IIT) under Project SEED "POLYPHEMO" and Regione Autonoma della Sardegna under L.R.7/2007. We thank the Visiting Professor program of Regione Sardegna. We acknowledge computational support by CYBERSAR (Cagliari, Italy), CINECA (Casalecchio di Reno, Italy), CASPUR (Rome, Italy), and the IIT Platform "Computation". We are also grateful to Claudio Melis for useful discussion and to Matteo Dessalvi for technical support.

#### ■ REFERENCES

- (1) Cummings, S. P.; Savchenko, J.; Ren, T. *Coord. Chem. Rev.* **2011**, *255*, 1587–1602.
- (2) Naaman, R. *Phys. Chem. Chem. Phys.* **2011**, *13*, 13153–13161.
- (3) Molina, J.; Fernández, J.; del Río, A.; Bonastre, J.; Cases, F. *Appl. Surf. Sci.* **2011**, *257*, 10056–10064.
- (4) Nabetani, Y.; Takamura, H.; Hayasaka, Y.; Shimada, T.; Takagi, S.; Tachibana, H.; Masui, D.; Tong, Z.; Inoue, H. *J. Am. Chem. Soc.* **2011**, *133*, 17130–17133.

- (5) Oosterhout, S. D.; Wienk, M. M.; van Bavel, S. S.; Thiedmann, R.; Koster, L. J. A.; Gilot, J.; Loos, J.; Schmidt, V.; Janssen, R. A. *Nat. Mater.* **2009**, *8*, 818–824.
- (6) Hsu, J. W.; Lloyd, M. T. *MRS Bull.* **2010**, *422*, 234701.
- (7) Özgür, U.; Alivov, Y.; Liu, C.; et al. *J. Appl. Phys.* **2005**, *98*, 1–103.
- (8) Zhao, J.-L.; Zhang, W.; Li, X.-M.; Feng, J.-W.; Shi, X. *J. Phys.: Condens. Matter* **2006**, *18*, 1495–1508.
- (9) Wang, Z. *J. Phys.: Condens. Matter* **2004**, *16*, R829–R858.
- (10) Kullkarni, A. J.; Zhou, M.; Ke, F. J. *Nanotechnology* **2005**, *16*, 2749–2756.
- (11) Blumstengel, S.; Koch, N.; Sadofev, S.; Schafer, P.; Glowatzki, H.; Johnson, R. L.; Rabe, J. P.; Henneberger, F. *Appl. Phys. Lett.* **2008**, *92*, 193303.
- (12) Martini, C.; Poize, G.; Ferry, D.; Kanehira, D.; Yoshimoto, N.; Ackermann, J.; Fages, F. *ChemPhysChem* **2009**, *10*, 2465–2470.
- (13) Mawrin, J.; et al. *J. Phys. Chem. C* **2011**, *115*, 10881–10888.
- (14) Garcia, R.; Tello, M.; Moulin, J.; Biscarini, F. *Nano Lett.* **2004**, *4*, 1115–1119.
- (15) Loi, M. A.; Da Como, E.; Dinelli, F.; Murgia, M.; Zamboni, R.; Biscarini, F.; Muccini, M. *Nat. Mater.* **2005**, *4*, 81–85.
- (16) Street, R. A. *Nat. Mater.* **2006**, *5*, 171–172.
- (17) Caddeo, C.; Melis, C.; Colombo, L.; Mattoni, A. *J. Phys. Chem. C* **2010**, *114*, 21109–21113.
- (18) Saba, M. I.; Melis, C.; Colombo, L.; Mattoni, A. *J. Phys. Chem. C* **2012**, *115*, 9651–9655.
- (19) Della Sala, F.; Blumstengel, S.; Hennerberger, F. *Phys. Rev. Lett.* **2011**, *107*, 146401.
- (20) Spallanzani, N.; Rozzi, C. A.; Varsano, D.; Baruah, T.; Pederson, M. R.; Manghi, F.; Rubio, A. *J. Phys. Chem. B* **2009**, *113*, 5345–5349.
- (21) Calzolari, A.; Ruini, A.; Catellani, A. *J. Am. Chem. Soc.* **2011**, *133*, 5893–5899.
- (22) Kohn, W.; Sham, L. *J. Phys. Rev.* **1965**, *140*, A1133–A1138.
- (23) Kanai, Y.; Grossman, J. C. *Nano Lett.* **2007**, *7*, 1967–1972.
- (24) Kanai, Y.; Grossman, J. C. *Nano Lett.* **2008**, *8*, 908–912.
- (25) Dag, S.; Wang, L.-W. *Nano Lett.* **2008**, *8*, 4185–4190.
- (26) Sai, N.; Leung, K.; Chelikowsky, J. *Phys. Rev. B* **2011**, *83*, 121309(R).
- (27) Wang, B.; Wang, X.; Chen, G.; Nagase, S.; Zhao, J. *J. Chem. Phys.* **2008**, *128*, 144710.
- (28) Wang, B.; Wang, X.; Zhao, J. *J. Phys. Chem. C* **2010**, *114*, 5741–5744.
- (29) De Angelis, F.; Armelao, L. *Phys. Chem. Chem. Phys.* **2011**, *13*, 467–475.
- (30) Persson, P.; Lunell, S.; Ojamäe, L. *Int. J. Quantum Chem.* **2002**, *89*, 172–180.
- (31) Lenz, A.; Selegård, L.; Söderlind, F.; Larsson, A.; Holtz, P. O.; Uvdal, K.; Ojamäe, L.; Käll, P.-O. *J. Phys. Chem. C* **2009**, *113*, 17332–17341.
- (32) Al-Sunaidi, A.; Goumri-Said, S. *Chem. Phys. Lett.* **2011**, *507*, 111–116.
- (33) Perdew, J. P.; Levy, M. *Phys. Rev. Lett.* **1983**, *51*, 1884–1887.
- (34) Bechstedt, F.; Del Sole, R.; Cappellini, G.; Reining, L. *Solid State Commun.* **1992**, *84*, 765–770.
- (35) Kümmel, S.; Kronik, L. *Rev. Mod. Phys.* **2008**, *80*, 3–58.
- (36) Jain, M.; Chelikowsky, J. R.; Louie, S. G. *Phys. Rev. Lett.* **2011**, *107*, 216806.
- (37) Onida, G.; Reining, L.; Rubio, A. *Rev. Mod. Phys.* **2002**, *74*, 601.
- (38) Hybertsen, M.; Louie, S. *Phys. Rev. B* **1986**, *34*, 5390–5413.
- (39) Blase, X.; Attaccalite, C.; Olevano, V. *Phys. Rev. B* **2011**, *83*, 115103.
- (40) Faber, C.; Attaccalite, C.; Olevano, V.; Runge, E.; Blase, X. *Phys. Rev. B* **2011**, *83*, 115123.
- (41) Jones, R. O.; Gunnarsson, O. *Rev. Mod. Phys.* **1989**, *61*, 689–746.
- (42) Gavnholt, J.; Olsen, T.; Engelund, M.; Schiøtz, J. *Phys. Rev. B* **2008**, *78*, 075441.
- (43) Kowalczyk, T.; Yost, S. R.; Voorhis, T. V. *J. Chem. Phys.* **2011**, *134*, 054128.

- (44) Malloci, G.; Mulas, G.; Cappellini, G.; Joblin, C. *Chem. Phys.* **2007**, *340*, 43–58.
- (45) Caddeo, C.; Dessi, R.; Melis, C.; Colombo, L.; Mattoni, A. *J. Phys. Chem. C* **2011**, *115*, 16833–16837.
- (46) Dmytruk, A.; Dmitruk, I.; Blonskyy, I.; Belosludov, R.; Kawazoe, Y. *Microelectron. J* **2009**, *40*, 218–220.
- (47) *TURBOMOLE V6.2 2010*, a development of University of Karlsruhe and Forschungszentrum Karlsruhe GmbH, 1989–2007, TURBOMOLE GmbH, since 2007; available from <http://www.turbomole.com>.
- (48) Perdew, J. P.; Burke, K.; Ernzerhof, M. *Phys. Rev. Lett.* **1996**, *77*, 3865–3868.
- (49) Weigend, F.; Ahlrichs, R. *Phys. Chem. Chem. Phys.* **2005**, *7*, 3297–3305.
- (50) Eichkorn, K.; Treutler, O.; Ohm, H.; Haser, M.; Ahlrichs, R. *Chem. Phys. Lett.* **1995**, *240*, 283–289.
- (51) Sierka, M.; Hogeckamp, A.; Ahlrichs, R. *J. Chem. Phys.* **2003**, *118*, 9136–9148.
- (52) Treutler, O.; Ahlrichs, R. *J. Chem. Phys.* **1995**, *102*, 346–354.
- (53) Tkatchenko, A.; Romaner, L.; Hofmann, O. T.; Zojer, E.; Ambrosch-Draxl, C.; Scheffler, M. *MRS Bull.* **2010**, *35*, 435–442.
- (54) Grimme, S. *J. Comput. Chem.* **2006**, *27*, 1787–1799.
- (55) Boys, S. F.; Bernardi, F. *Mol. Phys.* **1970**, *19*, 553–566.
- (56) Smith, W.; Todorov, I. T. *J. Mol. Graph.* **1996**, *14*, 136–141.
- (57) Ponder, J.; Case, D. *Adv. Protein Chem.* **2003**, *66*, 27–85.
- (58) Li, J.; Zhu, T.; Cramer, C. J.; Truhlar, D. G. *J. Phys. Chem. A* **1998**, *102*, 1820–1831.
- (59) Li, C.; Guo, W.; Kong, Y.; Gao, H. *Appl. Phys. Lett.* **2007**, *90*, 223102.
- (60) Meyer, B.; Marx, D. *Phys. Rev. B* **2003**, *67*, 035403.
- (61) Jirsak, T.; Dvorak, J.; Rodriguez, J. A. *J. Phys. Chem. B* **1999**, *103*, 5550–5559.
- (62) Mattioli, G.; Filippone, F.; Giannozzi, P.; Caminiti, R.; Bonapasta, A. A. *Chem. Mater.* **2009**, *21*, 4555–4567.

# Electronic Properties of Hybrid Zinc Oxide-Oligothiophenes Nanostructures

*(Supporting Information)*

Claudia Caddeo,<sup>\*,†,‡</sup> Giuliano Mallocci,<sup>‡</sup> Gian-Marco Rignanese,<sup>¶</sup> Luciano  
Colombo,<sup>†,‡</sup> and Alessandro Mattoni<sup>‡</sup>

*Dipartimento di Fisica Università di Cagliari, Istituto Officina dei Materiali del CNR, Unità  
Organizzativa di Supporto di Cagliari, Cittadella Universitaria, I-09042 Monserrato (Ca), Italy ,  
and Université Catholique de Louvain, B-1348 Louvain-la-Neuve, Belgium*

E-mail: claudia.caddeo@dsf.unica.it

---

\*To whom correspondence should be addressed

†University of Cagliari

‡CNR-IOM

¶Université Catholique de Louvain

In order to validate the overall computational scheme used, test calculations are performed on benzene, thiophene and ZnO dimer, for which experimental and accurate theoretical values are available. The results, summarized in Table 1, confirm the accuracy of the method employed.

**Table 1: Electron affinity (EA), ionization energy (IE) and HOMO-LUMO gap ( $E_g$ ) as given by DFT and  $\Delta$ SCF for benzene ( $C_6H_6$ ), thiophene ( $C_4H_4S$ ) and ZnO dimer, in comparison with Quantum Monte Carlo (QMC) and experimental (Exp.) data (values are in eV).**

	$C_6H_6$			$C_4H_4S$			ZnO		
	EA	IE	$E_g$	EA	IE	$E_g$	EA	IE	$E_g$
DFT	-1.17	6.29	5.13	-1.32	5.82	4.51	-5.70	5.12	0.59
$\Delta$ SCF	-1.57	9.25	10.81	-1.51	9.26	10.77	2.01	9.40	7.39
QMC <sup>a</sup>	-1.61	9.26	10.88	-1.55	8.99	10.55	—	—	—
Exp.	-1.12 <sup>b</sup>	9.24 <sup>c</sup>	10.36	<0.00	8.86 <sup>c</sup>	—	2.09 <sup>d</sup>	9.34 <sup>e</sup>	7.25

<sup>a</sup> from Ref. 1

<sup>b</sup> from Ref. 2

<sup>c</sup> from Ref. 3

<sup>d</sup> from Ref. 4

<sup>e</sup> from Ref. 5

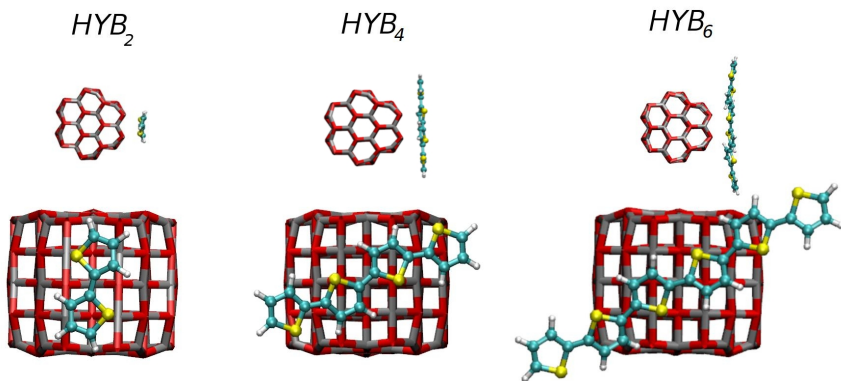


Figure 1: Top and side view of the three hybrids after the overall relaxing procedure. These geometries were obtained without taking into account the dispersive contributions.

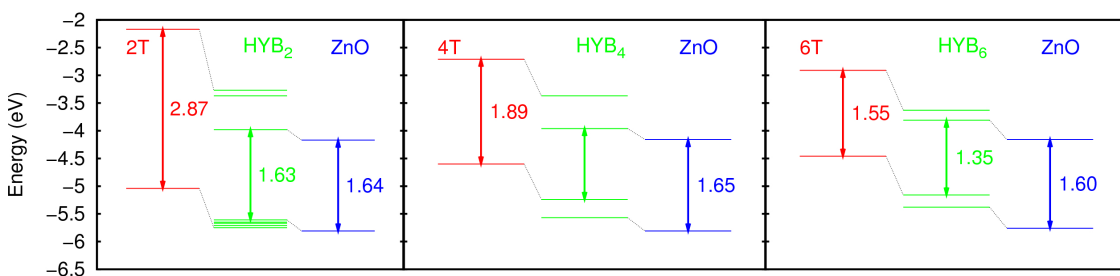
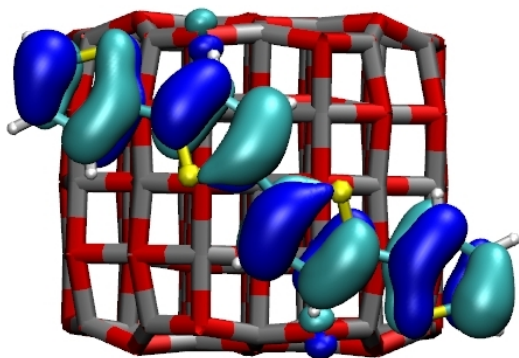


Figure 2: Correspondence between the DFT energy levels of the hybrids (green) and the levels of the separate moieties at the hybrid geometry (OT red,  $Zn_{60}O_{60}$  blue).

HOMO -5.24 eV



LUMO -3.96 eV

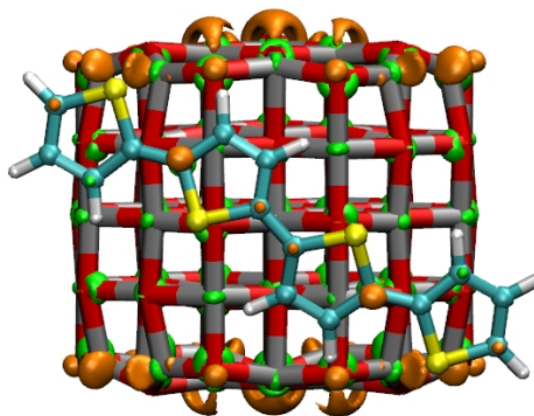


Figure 3: Spatial distribution of the HOMO (left, blue and cyan regions) and LUMO (right, orange and green regions) of the  $HYB_4$  system.

## References

- (1) Wu, Z.; Kanai, Y.; Grossman, J. C. *Phys. Rev. B* **2009**, *79*, 201309.
- (2) Burrow, P. D.; Michejda, J. A.; Jordan, K. D. **1987**, *86*, 9–24.
- (3) Lide, D. R. *CRC Handb. Chem. Phys.*, 89th ed.; CRC Press, Boca Raton, 2008.
- (4) Fancher, C. A.; de Clercq, H. L.; Thomas, O. C.; Robinson, D. W.; Bowen, K. H. *J. Chem. Phys.* **1998**, *109*, 8426–8429.
- (5) Clemmer, D. E.; Dalleska, N. F.; Armentrout, P. B. *J. Chem. Phys.* **1991**, *95*, 7263–7268.